Intermolecular Vibrational Coherence in Bacteriochlorophyll *a* with Clustered Polar Solvent Molecules

Katherine R. Shelly,[†] Elizabeth C. Golovich,[‡] and Warren F. Beck*

Department of Chemistry, Michigan State University, East Lansing, Michigan 48824

Received: May 11, 2006; In Final Form: August 10, 2006

We show that resonant impulsive excitation of the Q_y absorption band of bacteriochlorophyll *a* (BChl) launches a rapidly damped (γ < 200 fs) ground-state coherent wave-packet motion that arises from intermolecular modes with clustered solvent molecules. Femtosecond pump−probe, dynamic-absorption signals were obtained at room temperature with BChl solutions in pyridine, acetone, and 1-propanol. The vibrational coherence observed in the 0−800-fs regime is modeled in the time domain by two (or three, in the case of 1-propanol) modulation components with asymmetric, inhomogeneously broadened line shapes and frequencies in the 100−200-cm^{-1} range. The mean frequency of the vibrational coherence exhibits at least a quadratic dependence on the dipole moment of the solvent molecules and a *y*-intercept in the 100-cm^{-1} regime. This trend is modeled by an expression for the natural frequency of a "6−12" potential composed of attractive terms from van der Waals forces and a repulsive term from the exchange (Pauli exclusion) force. The model suggests that comparable contributions to the potential are provided by the dipole−dipole and London dispersion interactions. These results support the hypothesis that the low-frequency vibrational modes in the 100-cm^{-1} regime that are coupled to the light-driven charge-separation reactions in the reaction center from purple bacteria are derived from intermolecular vibrational modes between the chromophores and the surrounding protein medium.

Introduction

The primary and secondary charge-separation reactions in purple bacterial photosynthetic reaction centers exhibit essentially temperature-independent rates because the driving forces are almost exactly matched by reorganization energies in certain vibrational modes in the 100-cm^{-1} regime.[1] The structural origin of these coupled modes is indeterminate. Whether they are intramolecular normal modes, from the redox-active chromophores themselves, or from intermolecular interactions, between the chromophores and the surrounding protein structure, is crucial to the structural origin of the quantum efficiency of energy conversion.

At the forefront in the dynamics of the primary charge-separation reaction, the light-driven transfer of an electron from the paired-bacteriochlorophyll (BChl) primary electron donor, P, to the bacteriopheophytin acceptor, $BPhe_L$, are the vibrational modes that obtain enhanced resonance Raman intensity with excitation of P's lower-energy exciton-state absorption band. From photochemical hole-burning spectra obtained at cryogenic temperatures, Small and co-workers showed that a Franck−Condon progression along modes in the 125−150-cm^{-1} range accounts for most of the optical reorganization energy associated with the $\pi \rightarrow \pi^*$ transition.[2,3] Subsequently, Vos, Martin, and co-workers observed vibrational coherence in several modes over the 30−160-cm^{-1} range in femtosecond pump−probe transients with the probe tuned to the P* stimulated-emission band.[4−8] Stanley and Boxer[9] confirmed this assignment by detecting similar modulation frequencies in the weak fluorescence from P* using the femtosecond fluorescence upconversion method. The damping time for the coherent wave-packet motion on P*'s potential-energy surface is comparable to the electron-transfer time scale.[6] Considering that a transfer of population between the reactant P* and the product $P^+-BPhe_L^-$ surfaces would lead to a concomitant decrease in the amplitude of the P* wave packet, the possibility that the resonance Raman-active modes are the ones that are coupled to the electron-transfer reaction coordinate has been discussed.[10−16]

Several of the features in the <200-cm^{-1} region of P's resonance Raman spectrum are assigned by Bocian and co-workers to out-of-plane deformations of the BChl macrocycle.[17,18] These motions would modulate the strong electronic coupling and intramolecular charge-transfer properties of P,[19,20] so their involvement in promoting the primary electron-transfer process should be considered. In contrast, an assignment of the coupled modes to protein-derived motions was advanced in work by Vos, Martin, and co-workers. In reaction centers from *Rhodobacter sphaeroides*, at least seven active modes were detected in the vibrational coherence, with the strongest features observed in the 90−160-cm^{-1} range.[21] The lowest frequencies (10−30 cm^{-1}) in the set were assigned to *collective* protein-derived motions.[6] This suggestion was made in reference to the peak observed in the 50-cm^{-1} region of the vibrational density of states obtained from molecular dynamics simulations of small proteins;[22] a similar feature is observed in Raman spectra from protein crystals.[23] An analogous suggestion had already been made by Small and co-workers, who explicitly employed 30-cm^{-1} phonons in their analysis of the hole-burned spectra from P.[2,3]

Vos, Martin, and co-workers subsequently showed that the vibrational coherence from P* is perturbed by point mutations that alter hydrogen-bonding interactions between the BChl

[†] Current address: Beckman Coulter, Inc., 1000 Lake Hazeltine Blvd., Chaska, MN 55318.

[‡] Current address: Pacific Northwest Laboratories, P.O. Box 999, Mail Stop K5-25, Richland, WA 99352.

10.1021/jp062909v CCC: $33.50
Published on Web 09/16/2006

macrocycles and the surrounding protein. Especially because the mutations that affected the electronic configuration of P did not cause shifts of frequency,[24] and because a comparable vibrational coherence had not at that time been observed in solutions of BChl,[25,26] the active modes in the 90−160-cm^{-1} range were assigned not to the BChl macrocycles themselves but to the protein.[21,27]

An assignment of the protein character in the coupled modes that is consistent with these results would involve local intermolecular interactions between the redox-active macrocycles and polar groups in the surrounding protein structure. These interactions would be comparable to the van der Waals interactions between a chromophore and its clustered solvent molecules in condensed phases. As a group, these interactions are likely to exhibit mode frequencies in the critical 100-cm^{-1} regime inferred from the temperature dependence of the primary charge-separation reaction in reaction centers and from the studies of the associated vibrational coherence. In molecular liquids, intermolecular mode frequencies detected in nonresonant optical-Kerr-effect (OKE) experiments lie in the 10−200-cm^{-1} range;[28] collective motions of liquids are noted in the 10-cm^{-1} regime,[29] but pairwise interactions are found in the 60−100-cm^{-1} range.[30] Given that the modes with the clustered solvent molecules are likely to be displaced structurally by a change in the electron configuration of the redox-active chromophore, they should exhibit resonance Raman activity. In molecular solvents, the associated line shapes would be anticipated to be broad, like those observed in the OKE signals in liquids. In comparison, the line shapes from intermolecular modes in proteins might be expected to be sharper, more like those from those of the chromophore itself, owing to the higher degree of structural order.

Recent results from this laboratory are consistent with these hypotheses. Two distinct damping-time regimes were observed in the vibrational coherence exhibited by the dipyridine complex of BChl *a* in pyridine solvent. Over the 0−8-ps time scale, femtosecond pump−probe, dynamic-absorption transients obtained with impulsive excitation near the $\pi \rightarrow \pi^*$ spectral origin are weakly modulated by slowly damped components with damping times of $\gamma = 1.2-1.7$ ps and frequencies ranging over the 10−220-cm^{-1} regime; the spectral line shapes in the frequency domain from these components are relatively narrow ($\Delta\omega < 30$ cm^{-1}), which suggests an assignment to the intramolecular modes of the BChl macrocycle. A much more intense and very rapidly damped modulation, however, was observed on the <500-fs time scale; the broad spectral line shape of this component suggests an assignment to intermolecular modes between BChl *a* and the pyridine molecules in the first solvation shell.[31]

We focus in this contribution on the structural origin of the rapidly damped components of the vibrational coherence that can be observed in BChl solutions. We compare the rapidly damped vibrational coherence observed at room temperature in solutions of BChl *a* in pyridine, acetone, and 1-propanol. The results support an assignment of the vibrational coherence to intermolecular modes between BChl *a* and clustered solvent molecules in the first solvation shell because the mode frequency scales with the dipole moment of the solvent in a manner that is consistent with the natural frequency of a van der Waals bonding potential. This finding supports the hypothesis that intermolecular modes between solvent molecules and large electronic chromophores can have resonance Raman activity.

Experimental Section

BChl Solutions. Synthetically prepared BChl *a* was used as received from Frontier Scientific. Pyridine was obtained from Jade Scientific. Acetone was obtained from J. T. Baker. 1-Propanol was obtained from CCI. All of the solvents were of spectrophotometric grade.

Solutions of BChl *a* were manipulated in a glove bag under a dry N_2 atmosphere and in minimal light. The dry BChl powder was dissolved in solvent and then passed through a 0.22-μm filter. The concentration of the BChl solutions was adjusted with addition of neat solvent to obtain a final absorbance of 0.6−0.7 at 750 nm for a 1-mm path length.

Continuous-Wave Absorption and Fluorescence Spectra. Absorption spectra were obtained at 22 °C with a Hitachi U-2000 spectrometer (2-nm band-pass). Fluorescence spectra were acquired at 22 °C with a Hitachi F-4500 fluorescence spectrophotometer (5-nm band-pass for the excitation and emission monochromators). The fluorescence intensities were corrected using a calibration curve obtained from a standard lamp. As presented as a function of wavenumber, the fluorescence intensities are multiplied by the square of the wavelength in order to compensate for the fixed (in wavelength units) spectral band-pass of the emission spectrometer.[32,33]

Femtosecond Spectroscopy. Studies of vibrational coherence were performed with a pump−probe spectrometer consisting of a self-mode-locked Ti:sapphire oscillator, a prism-pair pulse compressor, and a rapid-scanning, modified Mach−Zehnder interferometer. These experiments employ the dynamic-absorption technique, a one-color pump−probe experiment with wavelength dispersion of the transmitted probe beam in a monochromator, which was first used with very short pulses by Shank, Mathies, and co-workers.[34−42] The use of ∼60-fs pulses and detection of a relatively narrow transmitted probe bandwidth in the present experiments is similar to the approach used by Champion and co-workers in their studies of low-frequency vibrational coherence in heme proteins.[43−45] Some of the apparatus and methodology has been described in previous work from this laboratory,[31,46,47] but some important changes are described in the following.

In this work, we used a Coherent Mira 900F Ti:sapphire oscillator and a Coherent Verdi Nd-YVO_4 pump laser (5-W version). The oscillator was equipped with Coherent's X-wave broad-tuning-range cavity optics. Extracavity group-delay precompensation was performed with a double-passed pair of SF10 Brewster-angled prisms; the separation between the prisms was adjusted to minimize the width of the zero-background autocorrelation function, as measured at the position of the sample. For the experiments reported in this paper, the autocorrelation width was ∼90 fs (fwhm); the spectral bandwidth was 11.5 nm.

In the Mach−Zehnder interferometer, the pump and probe beams were split from the *s*-polarized incident laser beam by a femtosecond autocorrelator beam splitter (CVI Laser, FABS-800-45S). The pump beam's intensity was modulated at 100 kHz by a $\lambda/2$-retarding photoelastic modulator (Hinds Instruments) followed by a calcite polarizer (Karl Lambrecht).[46] The pump−probe delay was scanned continuously by a ODL-150 galvanometer-driven delay line (Clark-MXR). A $\lambda/2$-retarding wave plate and a calcite polarizer, inserted in series in the probe beam, were oriented to obtain a 45° angle between the planes of linear polarization of the pump and probe beams. The two beams were focused by the same fused-silica lens (5-cm focal length) onto the sample's position.

The transmitted probe beam was analyzed by a calcite polarizer at 90° relative to the pump beam's plane of polariza-

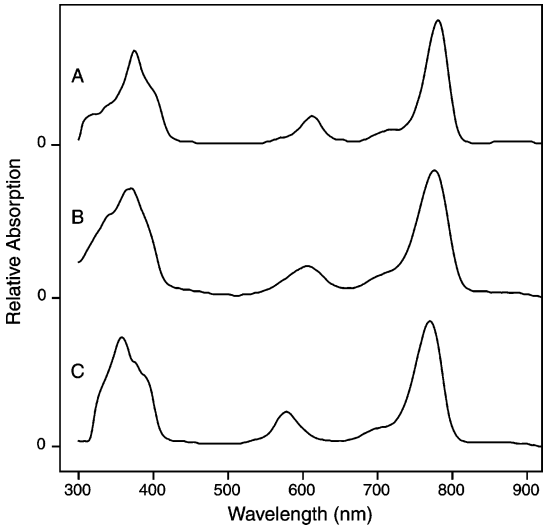

Figure 1. Continuous-wave absorption spectra at 22 °C from BChl *a* in three solvents: (A) pyridine, (B) 1-propanol, and (C) acetone.

tion, and then it was passed through a grating monochromator (Acton Research Spectra-Pro 150, 2-nm band-pass centered at 757 nm). The selected band-pass of the probe beam was detected by an amplified Si photodiode (Thorlabs PDA55). The photodiode's signal was processed by a lock-in amplifier (SRS, SR850) referenced to the 100-kHz pump-amplitude-modulation frequency; a differential detection scheme[31] was employed to remove common-mode laser noise. The analogue output of the lock-in amplifier was recorded and averaged using the sample/hold amplifier and digitizer system described previously.[47]

Samples were held at room temperature (22 °C) in a fused-silica flow cuvette (1-mm path length). A 10-mL reservoir of sample was pumped through the cuvette at 6 mL/min by a peristaltic pump. The sample's absorption spectrum was monitored during the experiment for changes arising from photochemistry or permanent photobleaching.

Results

Figure 1 shows the continuous-wave absorption spectra from BChl *a* dissolved in three solvents: pyridine, 1-propanol, and acetone. The spectra span the three absorption bands arising from $\pi \rightarrow \pi^*$ transitions: with increasing wavelength, the Soret or *B* band (~420-nm, $S_0 \rightarrow S_{n\geq 2}$ transitions), and the Q_x and Q_y bands (~600 nm and ~750 nm, $S_0 \rightarrow S_1$ transitions). In comparison to the spectrum in pyridine, the Q_y bands observed in 1-propanol and acetone are shifted to the blue, by 4 and 7 nm, respectively, owing to bulk solvatochromism. The Q_x band observed in acetone is shifted to the blue farther than would be expected by solvatochromism alone from the Q_x bands observed in pyridine and 1-propanol. Observation of the Q_x band for BChl *a* in the 610-nm region in pyridine and 1-propanol indicates that the Mg^{2+} ion is six-coordinate, with a solvent molecule ligated to each of the axial sites.[48] The 580-nm Q_x band observed in acetone, however, indicates that the Mg^{2+} ion is five-coordinate, with only a single acetone ligand bound to an axial site.[48−50]

The femtosecond dynamic-absorption transients reported in this paper were obtained with excitation of the Q_y absorption band. Figure 2 shows the Q_y-band absorption and fluorescence spectra of BChl *a* in pyridine at 22 °C. The spectra are plotted with respect to wavenumber ν as A/ν and F/ν^3, respectively, with normalization to unit area. The integrals of these quantities

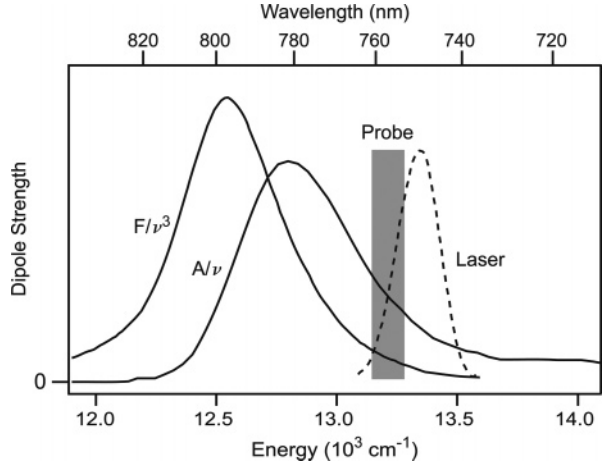

Figure 2. Q_y-band region of the continuous-wave absorption and fluorescence spectra from BChl *a* in pyridine, plotted as the dipole strength, A/ν and F/ν^3, respectively, and normalized to unit area. The Ti:sapphire oscillator's output spectrum (dashed curve) is superimposed with arbitrary scaling. The shaded region marks the 4-nm band-pass of transmitted probe light that was selected by the monochromator and passed to the detector in the femtosecond dynamic-absorption experiments.

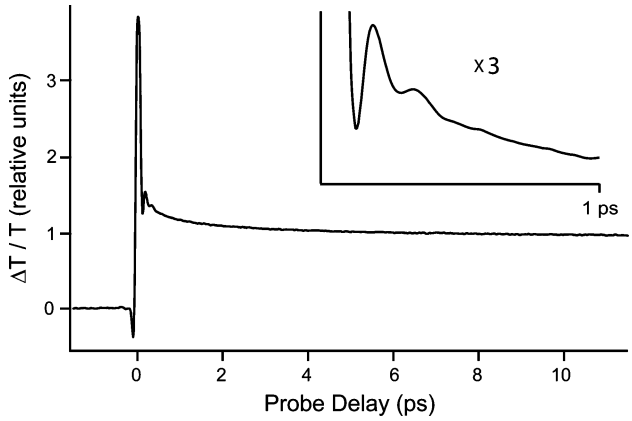

Figure 3. Dynamic-absorption transient from BChl *a* in pyridine. The inset shows a magnified view of the oscillatory portion of the signal.

report the dipole strength, the square of the transition-dipole moment.[32,51,52] Also shown in Figure 2 is the output spectrum from the Ti:sapphire oscillator. The shaded region marks the 4-nm band-pass of the transmitted probe spectrum that was passed by the monochromator to the photodiode. The pump spectrum and detected probe bandwidth specified in Figure 2 favors detection of ground-state vibrational coherence prepared by resonant impulsive stimulated Raman scattering (RISRS).[39,47,53] In our previous work on BChl *a* in pyridine,[31] however, the laser spectrum was tuned close to the 0−0 transition energy, where the absorption and fluorescence dipole-strength spectra cross. The detected probe bandwidth in those experiments overlaps significantly with the stimulated-emission spectrum, so ground-state and excited-state vibrational coherence were both likely to have made a contribution to the detected signals.

The dynamic-absorption transient obtained from BChl *a* in pyridine is shown in Figure 3. Following an intense spike[54−58] near the zero of time, the transient exhibits a short series of damped oscillations, with two strong recurrences prior to the 500-fs delay point. The first intense beat, at 200 fs, corresponds to the rapidly damped feature that we reported previously. Comparable modulations are observed in acetone and 1-propanol, as discussed below, over the 150−800-fs time range. A much weaker and more slowly damped set of oscillations is

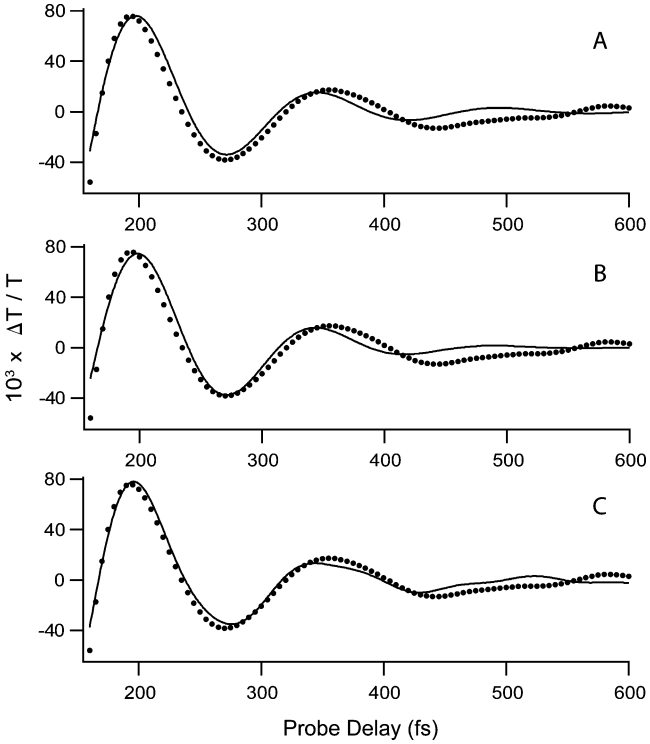

Figure 4. Expanded view of the rapidly damped oscillation observed in the dynamic-absorption transient from BChl *a* in pyridine (see Figure 3) and three optimized single-modulation-component models employing different line shapes: (A) a discrete $\omega = 225$ cm^{-1} cosinusoid (equation 1) with a damping time of $\gamma = 92$ fs, (B) a Gaussian distribution of damped cosinusoids with a center frequency of $\omega_0 = 225$ cm^{-1} and a width of $\Delta\omega = 50$ cm^{-1}, and (C) a log-normal distribution of damped cosinusoids with a center frequency of $\omega_0 = 285$ cm^{-1} and a width of $\Delta\omega = 97$ cm^{-1}. The models for parts B and C were defined by eq 2, with the distributions $\mathcal{A}(\omega)$ set as a Gaussian and as a log-normal, respectively. The scaling of the ordinate is relative to the magnitude of the pump−probe ground-state depletion signal, as indicated in Figure 3.

readily observed in pyridine out at least to the 8-ps delay point.[31] The slowly damped signals are perhaps a factor of 5 weaker in acetone or 1-propanol than observed in pyridine.

The oscillations observed over the 150-fs−12-ps time range arise from *resonant* vibronic excitation of the BChl *a* molecules. As we discussed previously,[31] the nonresonant optical-Kerr-effect (OKE) signal from the pyridine solvent is weak in comparison to the BChl signal under the excitation and polarization conditions used in these experiments. Note that the OKE signals from acetone and 1-propanol are much weaker than that from pyridine. The OKE signals are further attenuated by the inner-filter effect[58,59] in the presence of the BChl *a* solute. To avoid any contributions from solvent-derived background signals,[58] we discard the signal that falls prior to the 100-fs delay point. In the following, we present a time-domain modeling of the rapidly damped oscillatory signals from BChl *a* in pyridine (Figures 4 and 6), acetone (Figure 7), and 1-propanol (Figure 8). In each case, the oscillatory signal was isolated from the overall signal (such as that in Figure 3) by subtracting a fitted triple-exponential decay function from the signal starting at 150 fs and extending to the end of the recording at 12 ps.

Figure 4 shows a series of preliminary models that attempt to describe the oscillatory signal obtained with BChl *a* in pyridine with a single modulation component. Figure 4A shows that a damped cosinusoid with frequency $\omega = 225$ cm^{-1},

$$I(t) = I_0 \cos(wt - \phi)e^{-t/\gamma} \qquad (1)$$

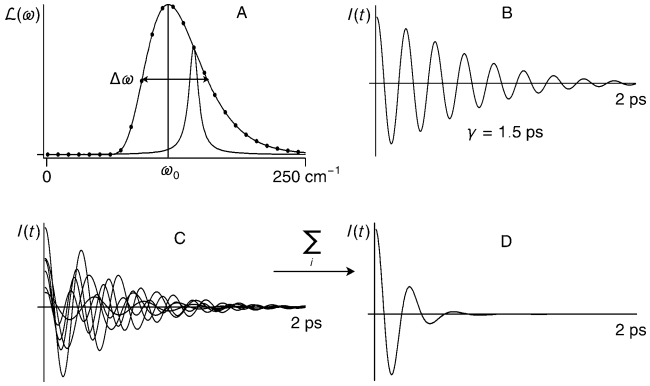

Figure 5. Modeling the rapidly damped vibrational coherence observed in BChl *a* solutions with a distribution of slowly damped cosinusoids, $\mathcal{A}(\omega)$, as defined by eq 2. A log-normal distribution $\mathcal{A}(\omega)$ (A), defined by its center frequency, ω_0, width, $\Delta\omega$, and asymmetry (or skew), ρ, is sampled over its full width. Each sample defines the intensity of a Lorentzian line shape that corresponds in the time domain (B) to a cosinusoid at the sampled frequency ω with an intrinsic damping time γ, here set arbitrarily to 1.5 ps. Summing of the cosinusoids obtained by sampling over the full width of the distribution $\mathcal{A}(\omega)$ (C) results in a rapidly damped waveform (D) that resembles the vibrational coherence observed in BChl solutions.

is capable of roughly describing only the first beat in the signal; the damping time ($\gamma = 92$ fs) defines a very broad Lorentzian line shape in the frequency domain ($\Delta\omega = 362$ cm^{-1}).[52] The second beat in the model is significantly phase shifted with respect to that of the experimental signal, and a large deviation of the model and signal is observed at delays >400 fs.

A better description of the oscillatory signal from BChl *a* in pyridine is obtained from an integral over a distribution of damped cosinusoids,

$$I(t) = \int_0^\infty d\omega\, \mathcal{A}(\omega,A,\omega_0,\Delta\omega,\rho) \cos(\omega t - \phi)e^{-t/\gamma} \qquad (2)$$

which can be implemented computationally as a sum of discrete cosinusoids (eq 1), as shown in Figure 5. The intensity $\mathcal{A}(\omega)$ for a cosinusoid of frequency ω is determined here by a log-normal distribution, as parametrized by its area (A), center frequency (ω_0), width ($\Delta\omega$), and asymmetry ($\rho > 1$).[60] These parameters were specified as adjustable parameters in a non-linear regression routine for the pro Fit 6.0 program; the robust (grid-search) optimization algorithm was employed in this work.[61] For Figure 4B, ρ was fixed to unity in order to obtain a Gaussian line shape. In Figure 4C, an asymmetric line shape was obtained by allowing ρ to float; in Table 1, we use the sign of ρ to indicate whether the broader side of the optimized line shape is directed to high ($\rho > 1$) or low frequency ($\rho < 1$). The tabulated values for the area A report the integral from zero frequency over the distribution $\mathcal{A}(\omega)$,

$$A = \int_0^\infty d\omega\, \mathcal{A}(\omega) \qquad (3)$$

For the multicomponent models that will be described next, the A values are normalized so that they sum to unity for the signal in pyridine; the A values reported for the signals in the other two solvents are normalized by the same scaling factor used for pyridine, so they report the relative modulation intensity compared to that of the signal in pyridine.

The intrinsic damping time γ was arbitrarily fixed in all models to 1.5 ps, in the range of the damping times for the slowly damped modulation features we observed for BChl *a* in

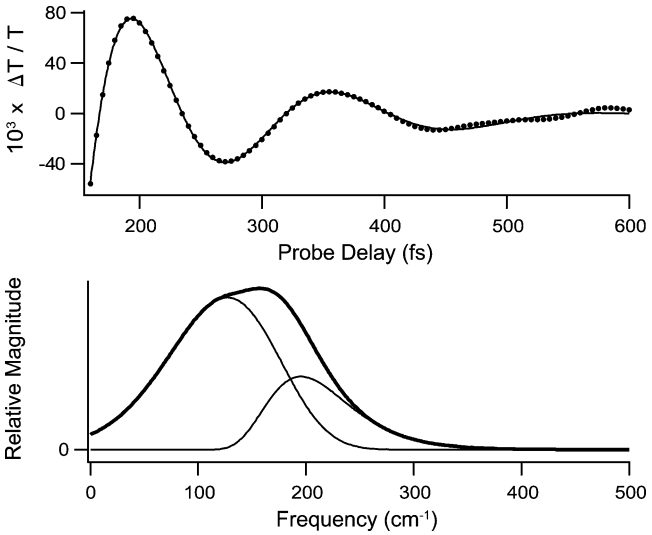

Figure 6. Expanded view of the rapidly damped oscillation observed in the dynamic-absorption transient from BChl *a* in pyridine (see Figures 3 and 4) superimposed with a model defined by the sum of two independent log-normal distributions $\mathcal{A}(\omega)$ of damped cosinusoids, each defined by eq 2. The scaling of the ordinate is relative to the magnitude of the pump−probe ground-state depletion signal, as in Figure 3. Bottom: Plots of $\mathcal{A}(\omega)$ for the two components observed in pyridine and their sum, $\mathcal{M}(\omega)$ (thick curve). The model parameters are provided in Table 1.

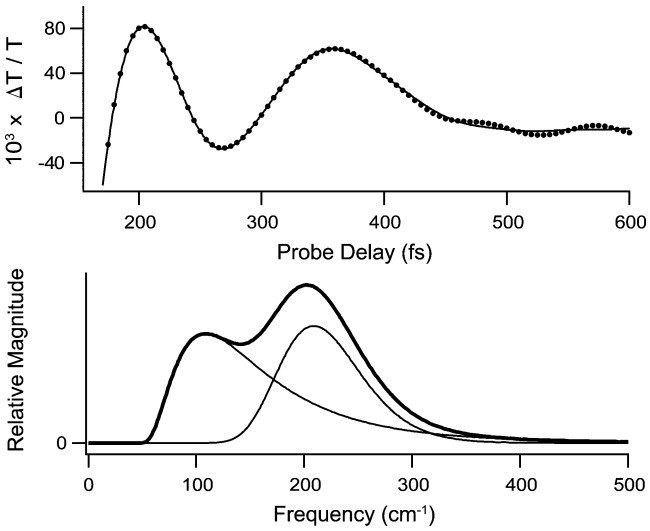

Figure 7. Expanded view of the rapidly damped oscillation observed in the dynamic-absorption transient from BChl *a* in acetone superimposed with a model defined by the sum of two independent log-normal distributions $\mathcal{A}(\omega)$ of damped cosinusoids, each defined by eq 2. The scaling of the ordinate is relative to the magnitude of the pump−probe ground-state depletion signal, as in Figure 3. Bottom: Plots of $\mathcal{A}(\omega)$ for the two components observed in acetone and their sum, $\mathcal{M}(\omega)$ (thick curve). The model parameters are provided in Table 1.

pyridine[31] and for the carbocyanine dye IR144 in polar solution.[47] The optimized fit to the oscillatory signal is not strongly dependent on the choice of γ in any case. Similar line shapes are obtained for $\mathcal{A}(\omega)$ when longer damping times are specified; for a fit to a given oscillatory signal, the width of the distribution gets narrower as γ is shortened. The sum of discrete cosinusoids (eq 2) converges satisfactorily with $\gamma = 1.5$ ps when $\mathcal{A}(\omega)$ is sampled at 5-cm^{-1} intervals over the 1−500-cm^{-1} range. Modulation frequencies of $\omega > 500$ cm^{-1} are not impulsively excited to a significant degree by the 60-fs pump pulses employed in the present experiments, so the sum can be truncated at that point without any discernible impact on the fit.

The fit obtained from the asymmetric distribution (Figure 4C) does a better job of describing the first and second beats in the signal than the fits obtained from the Lorentzian and Gaussian distributions (Figure 4A and B). All three models fail, however, to describe accurately the signal's rising trend before the first beat, at delays <200 fs, and each exhibits a weaker third beat, centered at the 480-fs delay point, that the experimental signal lacks. This analysis suggests that a more elaborate model, with at least two independent components, is required to describe the signal satisfactorily. Figure 6 shows that an excellent description of the oscillatory signal from BChl *a* in pyridine can be obtained from a sum of two distributions of damped cosinusoids. Both distributions were defined by eq 2; each was allowed to have an independent phase ϕ and asymmetry ρ. The optimized log-normal components are centered at 121 and 205 cm^{-1}.

A similar analysis was performed with the oscillatory signals obtained from BChl *a* in acetone and 1-propanol solutions. Preliminary models (not shown) were obtained with single damped cosinusoids (eq 1); a 251-cm^{-1} cosinusoid ($\gamma = 65$ fs; $\Delta\omega = 513$ cm^{-1}) provided the best fit to the signal in acetone, while a 208-cm^{-1} cosinusoid ($\gamma = 144$ fs; $\Delta\omega = 231$ cm^{-1}) was the best fit for the signal in 1-propanol. As in pyridine, these models deviate from the observed signals beyond the first beat.

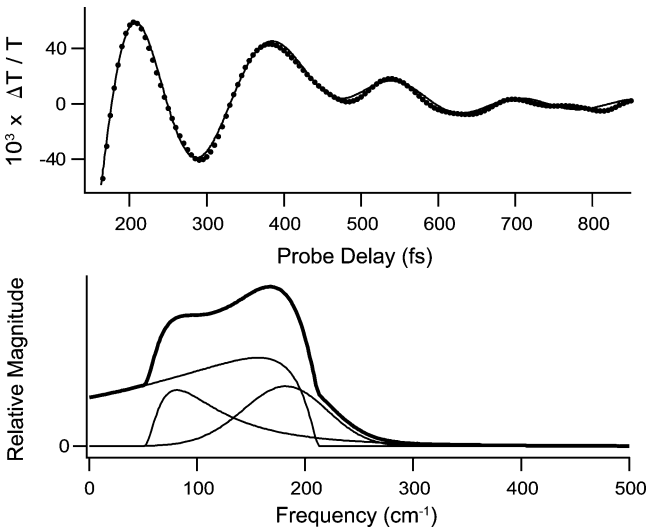

Figure 8. Expanded view of the rapidly damped oscillation observed in the dynamic-absorption transient from BChl *a* in 1-propanol superimposed with a model defined by the sum of three independent log-normal distributions $\mathcal{A}(\omega)$ of damped cosinusoids, each defined by eq 2. The scaling of the ordinate is relative to the magnitude of the pump−probe ground-state depletion signal, as in Figure 3. Bottom: Plots of $\mathcal{A}(\omega)$ for the three components observed in 1-propanol and their sum, $\mathcal{M}(\omega)$ (thick curve). The model parameters are provided in Table 1.

Figure 7 shows that a sum of two distributions of damped cosinusoids, one centered at 108 cm^{-1} and the other at 210 cm^{-1}, provides a very good description of the signal from BChl *a* in acetone. This signal differs from the one observed in pyridine most obviously in having a more intense and wider second beat.

The oscillatory signal observed from BChl *a* in 1-propanol can be distinguished from the ones observed in the other solvents in having four relatively strong beats on the <800-fs time scale; the signals observed in pyridine and acetone exhibit only two strong beats that are confined to the <500-fs regime. Figure 8 shows that a sum of three distributions of damped cosinusoids

TABLE 1: Model Parameters for the Rapidly Damped Vibrational Coherence Observed in Bacteriochlorophyll *a* Solutions[a]

		solvent		
component	parameter[b]	pyridine	acetone	1-propanol
1	ω_0, cm^{-1}	127	108	81
	$\Delta\omega$, cm^{-1}	120	109	25
	ρ	−1.1	1.7	1.2
	ϕ, rad	−0.178	0.329	0.398
	A	0.725	0.326	0.095
2	ω_0, cm^{-1}	195	210	182
	$\Delta\omega$, cm^{-1}	91	92	63
	ρ	1.3	1.2	−1.1
	ϕ, rad	−0.041	1.713	0.194
	A	0.275	0.406	0.106
3	ω_0, cm^{-1}			165
	$\Delta\omega$, cm^{-1}			426
	ρ			−2.4
	ϕ, rad			3.036
	A			0.263
sum	$\langle\omega\rangle$, cm^{-1}	146	189	131
	$\sum_i A_i$	1.000	0.732	0.465

[a] Figures 6−8. [b] See eqs 2−5 and the text.

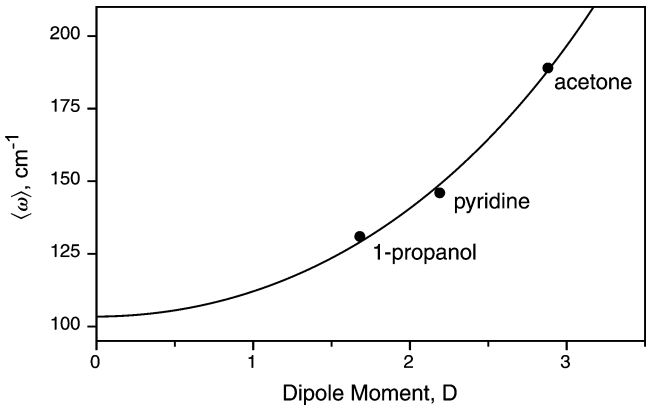

Figure 9. Solvent dependence of the mean frequency, $\langle\omega\rangle$, of the rapidly damped vibrational coherence observed in BChl *a* solutions (Figures 6−8). The ordinate was calculated from the sum of the fitted modulation components, $\mathcal{M}(\omega)$, using eq 5; the abscissa is the gas-phase dipole moment of the solvent.[62] The data points are superimposed with a model curve (eq 8) derived from an expression for the natural frequency (eq 7) for the 6−12 potential for the BChl−solvent intermolecular mode.

provides a good description of the signal; a model with only two components (not shown) describes only the first two beats. Two of the modulation components, with distributions centered at 66 and 171 cm^{-1}, are comparable to the pair observed in the other solvents. The third, the most intense component of the three, extends from its maximum at 165 cm^{-1} all the way down to 0 cm^{-1}.

The model parameters for the rapidly damped vibrational coherence from BChl *a* observed in the three solvents are compared in Table 1. A better sense of how the vibrational coherence depends on the choice of solvent can be obtained from an analysis of the mean frequency of the fitted distributions,

$$\langle\omega\rangle = \frac{\int_0^\infty d\omega\ \mathcal{M}(\omega)\omega}{\int_0^\infty d\omega\ \mathcal{M}(\omega)} \tag{4}$$

with the integral calculated over the ω axis with the sum of the distributions $\mathcal{M}(\omega)$ from the two or three components,

$$\mathcal{M}(\omega) = \sum_i \mathcal{M}_i(\omega) \tag{5}$$

Figure 9 shows that $\langle\omega\rangle$ exhibits at least a quadratic trend with respect to the gas-phase dipole moment[62] of the solvent; the *y*-intercept of the trend is in the 100-cm^{-1} regime.

Discussion

The results presented in this paper show that resonant impulsive excitation of the lowest $\pi \rightarrow \pi^*$ transition of BChl *a* initiates a rapidly damped coherent vibrational motion that depends strongly on the choice of solvent. An assignment of the vibrational coherence to solvent−BChl *intermolecular* modes that are coupled to the BChl $\pi \rightarrow \pi^*$ transition is indicated by the following observations:

(1) The dependence of the mean frequency of the vibrational coherence on the dipole moment of the solvent is consistent with a relation for the natural frequency of an intermolecular bonding potential that includes attractive terms from van der Waals forces.

(2) The mean frequencies and line widths of the components in the vibrational coherence are comparable to those associated with intermolecular modes in pure liquids, as observed in OKE experiments.[28−30,63−68]

In the following, we consider first the structural issues that control the resonance Raman activity of intermolecular modes with BChl molecules, and then the solvent dipole-moment dependence of the natural frequency of an intermolecular potential is derived. We examine next the nature of the broad line shapes that are observed in the vibrational coherence and the distinction between the line shapes for intermolecular and intramolecular vibrational coherence. We conclude with some comments on the nature of the vibrational coherence in the photosynthetic reaction center and on the optimization of the charge-separation dynamics by intermolecular interactions with the BChl macrocycles.

Structural Assignments. As shown in Figure 2, the tuning of the pump-laser spectrum and of the transmitted probe bandwidth favors detection of coherent wave-packet motion on the ground-state potential-energy surface. The wave packets are prepared and launched on the ground-state surface by the resonant impulsive stimulated Raman scattering mechanism.[39,47,53] An observation of resonance Raman activity in intermolecular modes between BChl *a* and solvent molecules under our excitation conditions suggests that the solvent molecules that contribute to the signal are structurally displaced by the $\pi \rightarrow \pi^*$ transition, so these molecules are in direct contact with the π-electron density of the BChl macrocycle. We assume here that the active modes are those for which the Albrecht *A* term is large; the *B*-term active modes are those that mix the Franck−Condon electronic state with nearby states to lower energy, so they have dominant activity with preresonance excitation.[69−73]

We are aware of only a few attempts to detect intermolecular modes in condensed phases using resonance Raman spectroscopy in the frequency domain. Mathies and co-workers observed resonance Raman-active modes from alcohol[74] and water[75] solutions of the solvated electron. The solvated electron is a diffuse structure that makes a significant ground-to-excited-state change in size and shape;[76−80] it apparently interacts strongly enough with a number of molecules in its first solvation shell that the absorption transition is vibronically coupled to a number of the solvent's high-frequency intramolecular modes.[74,75] The

lowest frequency resonance-enhanced modes observed in water, at 110 cm^{-1}, are assigned to the intermolecular modes between the electron and molecules in the first solvation shell.[75] In contrast, Waterland and Kelley[81] did not observe features from intermolecular modes in their UV resonance Raman studies of the nitrate ion in several solvents, but the π-electron density of the nitrate ion is highly localized. A similar localization might be responsible for the lack of detection of intermolecular modes in the femtosecond pump−probe studies of the cyanide-bridged $Ru^{II,III}$ mixed-valence complex by Barbara and co-workers. Significant solvent dependences were noted in the intervalence charge-transfer rate and in the damping of the ground-state vibrational coherence, but none of the modulation components were assigned to intermolecular modes.[82]

A consideration of this background prompts the hypothesis that $\pi \rightarrow \pi^*$ transitions in chromophores with delocalized π-electron density, such as the chlorophylls and porphyrins, might exhibit vibronic coupling to intermolecular modes with the small number of first-shell solvent molecules that are *clustered*[83,84] with it owing to specific structural interactions. Displacement of the intermolecular mode would be mediated by a change in the shape and extent of the π-electron density owing to the $\pi \rightarrow \pi^*$ change in electron configuration. Note that similar mode displacements might be driven by electron-transfer reactions, since the redox-active electrons are usually associated with the frontier molecular orbitals. The semicontinuum theory for electron-transfer reactions described by Mikkelsen and Ratner[85−87] involves a comparable structural picture: a small number of clustered solvent molecules in the first solvation shell surrounded by a dielectric continuum.

We suggest that the resonance Raman-active interactions with BChl *a* involve interactions of a solvent molecule with the π-electron density above or below the plane of the macrocycle. These interactions might resemble those in liquid pyrrole, where one pyrrole molecule makes a perpendicular attack on the π-electron density of an adjacent molecule,[88] yielding intermolecular modes in the 100-cm^{-1} region.[89] A similar T-shaped configuration is observed in benzene crystals,[90,91] but recent ab initio calculations suggest that a displaced parallel configuration is somewhat more stable for the benzene−benzene[92] and hexafluorobenzene−benzene[93] interactions in the gas phase, and a similar conclusion is made for pairwise interactions of larger polycyclic aromatic hydrocarbons.[94,95] An alternative configuration for the interaction of pyridine and possibly acetone with BChl, then, would involve a parallel, π-stacking attack.

Support for the attack of clustered solvent molecules on the π-electron density of the BChl macrocycle can be taken from the work of Kincaid and co-workers,[96,97] who observed resonance Raman intensity enhancement of a high-frequency intramolecular mode from solvent toluene molecules when the Soret absorption band of the dioxygen complex of a cobalt porphyrin was excited. This intensity enhancement was assigned to vibrational coupling of the toluene mode with the O−O stretching mode of the axially ligated O_2 molecule. Here, the approximate matching of the O_2 stretching frequency with the intrinsic frequency of the toluene mode allows mixing of the two modes, so the enhanced Raman intensity for the toluene line is borrowed from that of the O_2 line, and a small splitting between the two mixed Raman lines is the result. Such a mixing requires a first-shell interaction between the solvent toluene and the cobalt porphyrin complex. In fact, Kincaid and co-workers[96] showed that the O−O stretching mode of the dioxygen complex of a cobalt "picket-fence" porphyrin, which was protected on the O_2-binding face of the porphyrin by sterically bulky groups, was decoupled from the toluene modes.

Although a chemical origin from distinct configurations or sites for the binding of solvent molecules on the BChl macrocycle might also be considered, a general assignment for the two overlapping distributions observed in the vibrational coherence in the three solvents (see Figures 6−8) involves the hindered translational and rotational (librational) modes. Instantaneous normal-mode calculations from molecular dynamics simulations of polar liquids produce overlapping distribution functions for the translational and rotational modes that are quite similar in appearance to the ones we obtain from the BChl solutions, with the maximum of the translational component appearing at a lower frequency than that of the rotational component.[98,99]

The model for the signal in 1-propanol (see Figure 8) includes an additional, very broad component that exhibits significant intensity all the way to 0 cm^{-1}. This ultra-low-frequency character is not observed in the other two solvents (see Figures 6 and 7). We suggest that this component of the vibrational coherence arises from hydrogen-bonded chains[100−103] of 1-propanol molecules that are coupled to a given BChl macrocycle. This suggestion accounts for the lack of such a low-frequency character in the vibrational coherence in pyridine and acetone solvents because these solvents lack the ability to form intermolecular hydrogen bonds that would lead to formation of chains of molecules.

Intermolecular Potentials and Mode Frequencies. In the following, we consider how the frequency of the intermolecular mode between a BChl molecule and a clustered solvent molecule should depend on the latter's dipole moment through a discussion of the general properties of the intermolecular potential. The potential (V) as a function of the intermolecular distance (r) should have the form of a "6−12" potential in which the attractive $1/r^6$ part arises from van der Waals interactions:

$$V(r) = a/r^{12} - (b\alpha_1\alpha_2 + c|\boldsymbol{\mu}_1|^2|\boldsymbol{\mu}_2|^2 + \alpha_2|\boldsymbol{\mu}_1|^2 + \alpha_1|\boldsymbol{\mu}_2|^2)/r^6 \quad (6)$$

Following the a/r^{12} term, which describes the steep repulsive potential associated with the exchange (Pauli exclusion) force, there are a series of attractive terms that are scaled by $1/r^6$. The constant $b = 3I_1I_2/2(I_1 + I_2)$, with $I_{1,2}$ representing the ionization energies for the two molecules, scales the term with the polarizabilities ($\alpha_{1,2}$) from the London dispersion force. The constant $c = 2/3k_BT$, with k_B and T representing the Boltzmann constant and the temperature, respectively, scales the term from the dipole−dipole interaction; $\boldsymbol{\mu}_{1,2}$ are the dipole moments for the two interacting molecules. The high-temperature limit, where k_BT is much larger than the interaction energy, is assumed; the interaction is averaged over all orientations. The last two terms arise from the dipole−induced-dipole (Debye induction) interactions, so they are described by the products of the polarizability for one molecule and the square of the dipole moment for the other molecule.[104−107]

The first two terms of a Taylor series expansion of the intermolecular potential at its minimum yields expressions for the depth of the potential well and for the dependence of the potential on the square of the displacement. With the assumption of small displacements relative to the equilibrium geometry, one obtains an expression for the force constant (k) of the oscillator by equating the second term of the series to the Hooke's law potential for a harmonic oscillator, $V = kr^2/2$. The natural frequency of the harmonic oscillator is $\nu = (1/2\pi)(k/\mu)^{1/2}$, with μ standing here for the reduced mass,[52] so from the

force constant we obtain an expression for the frequency for the intermolecular mode,

$$\nu = C(b\alpha_1\alpha_2 + c|\boldsymbol{\mu}_1|^2|\boldsymbol{\mu}_2|^2 + \alpha_2|\boldsymbol{\mu}_1|^2 + \alpha_1|\boldsymbol{\mu}_2|^2)^{7/6}/2\pi\mu^{1/2} \quad (7)$$

with the constant $C = 3/(2a)^{2/3}$.

For an application of this result to the BChl−solvent intermolecular mode, let us assign the subscripts 1 and 2 to the BChl molecule and the solvent molecule, respectively. Holding all the other parameters constant in order to obtain an approximate expression that can be plotted, the frequency of the intermolecular mode should depend on the dipole moment of the solvent molecule according to the following relation

$$\nu = C_1 + C_2|\boldsymbol{\mu}_2|^{7/3} \quad (8)$$

where the constant C_1 includes contributions from the London dispersion interaction and from the induction term for the solvent (from $\alpha_2|\boldsymbol{\mu}_1|^2$); the constant C_2 includes contributions from the induction term for the BChl molecule (from $\alpha_1|\boldsymbol{\mu}_2|^2$) and the dipole−dipole interaction term. Given that the induction terms are usually smaller than the other terms in the potential,[104−107] the main contributions to the two terms are likely to be from the London dispersion and dipole−dipole terms, respectively.

Figure 9 shows a fit of eq 8 to the observed mean frequencies from the vibrational coherence observed in the three solvents. From the curving trend of the mean frequency as the dipole moment of the solvent is varied, it is obvious that a significant part of the binding interaction involves the sum of the dipole−dipole and solvent−dipole induction terms. The extension of the curve to a *y*-intercept in the 100-cm^{-1} regime suggests that the London dispersion interaction and the BChl−dipole induction terms make at least a comparable contribution.

Line Shapes for Intermolecular and Intramolecular Modes in Solution and Proteins. The femtosecond time-domain methods used in the present work are likely to be uniquely capable of detecting resonance Raman-active intermolecular modes in delocalized π-electron systems because the line shapes are very broad. In the time domain, broad line shapes result in sharp, rapidly damped features in the vibrational coherence, and the signal can be resolved into components on the basis of their distinct *phases*. We modeled the line shapes in the time domain using inhomogeneously broadened distributions (see eq 2); given the nature of the model, it is natural to suggest that the breadth of the line shapes arises from structural disorder in the chromophore−solvent interaction. Similar broad line shapes are observed in *nonresonant* OKE experiments in liquids,[28−30,63−68] but the Raman-active modes detected in the present experiments arise from *resonant* excitation of the BChl $\pi \rightarrow \pi^*$ transition. In a redox protein, the intermolecular modes between a chromophore and its surroundings might be expected to exhibit sharper line shapes because the interaction would be much more ordered than in a liquid.

As we noted in our previous report,[31] the rapidly damped vibrational coherence observed in BChl *a* in pyridine exhibits a much stronger signal in the time domain than is associated with the slowly damped vibrational coherence that extends at least to the 8-ps delay point. We assign the slowly damped signals to vibrational modes that are predominantly intramolecular in character, involving mostly motions of the BChl macrocycle only. The damping times of these signals are in the 1.2−1.7-ps range, corresponding to <30 cm^{-1} line widths in the frequency domain. These widths are not much broader than the Raman line widths of small molecular liquids, where inhomogeneous broadening causes perhaps a doubling of the width over that of the homogeneous line shape.[108] We noted above that this slowly damped vibrational coherence is much weaker in the acetone and 1-propanol solutions. The most likely explanation for these observations involves a different strength of electronic interaction between the axial ligands and the π-electron density of the BChl macrocycle. When pyridine is ligated, this interaction mixes some of the strong high-frequency resonance Raman activity in the plane of the macrocycle into the low-frequency, out-of-plane deformation modes that are visible in the <300-cm^{-1} region of the spectrum.[17,18] Our results show that the axially ligated acetone and 1-propanol molecules do not interact nearly as strongly as pyridine does with the π-electron density of the BChl macrocycle, so a lower degree of mixing of activity into the out-of-plane modes is the result.

Role of Intermolecular Modes in Photosynthesis. The work described in this paper provides a new perspective on the structural origin of the vibrational modes that control the dynamics of electron transfer in purple bacterial reaction centers. In solution, the intermolecular modes between BChl *a* and its clustered polar solvent molecules make a dominant contribution to the low-frequency vibrational coherence. The fitted trend for the dependence of the mean frequency as a function of the solvent's dipole moment (see Figure 9) suggests that a resonance Raman-active interaction with a natural frequency in the 100-cm^{-1} range should be expected with BChl solutes even in the limit of nonpolar media. The London dispersion term and the BChl−dipole induction term are the only active terms in the intermolecular potential (eq 6) in the nonpolar limit.

The addition of a few polar groups in contact with the π-electron density of a BChl macrocycle would tune the average mode frequency to a higher frequency. The perturbations in mode frequency that were observed in the site-directed mutagenesis studies by Vos, Martin, and co-workers[21,27] probably arise from changes in number and interaction strength of dipole−dipole or hydrogen-bonding interactions with the polar side chains of amino acids in the vicinity of the primary electron donor, P. These interactions are likely to be the ones that tune the reorganization energy so that it nearly matches the driving force for the charge-separation reaction. Reorganization of the protein medium, through polar and nonpolar solvation responses,[33,109,110] would be expected to play an additional, energy dissipative role in the dynamics that affords additional control over the reversibility of the charge-separation reactions. These ideas can be tested in experiments that probe the nature of the line shape and the mode frequency for the intermolecular mode in protein hosts. There are also a number of implications for the dynamics of electron transfer and the conformational change of chromophores in proteins that deserve consideration in future work.

Acknowledgment. This project was supported by the National Science Foundation Molecular Biophysics program under grants MCB-009120 and MCB-0520002. Additional support for instrumentation was provided by the Michigan Structural Biology Center at Michigan State University, which is supported by the Michigan Life Sciences Corridor.

References and Notes

(1) Bixon, M.; Jortner, J. *Chem. Phys. Lett.* **1989**, *159*, 17−20.
(2) Johnson, S. G.; Tang, D.; Jankowiak, R.; Hayes, J. M.; Small, G. H. *J. Phys. Chem.* **1989**, *93*, 5953−5957.
(3) Johnson, S. G.; Tang, D.; Jankowiak, R.; Hayes, J. M.; Small, G. J.; Tiede, D. M. *J. Phys. Chem.* **1990**, *94*, 5849−5855.
(4) Vos, M. H.; Lambry, J. C.; Robles, S. J.; Youvan, D. C.; Breton, J.; Martin, J. L. *Proc. Natl. Acad. Sci. U.S.A.* **1991**, *88*, 8885−8889.

(5) Vos, M. H.; Lambry, J. C.; Robles, S. J.; Youvan, D. C.; Breton, J.; Martin, J. L. *Proc. Natl. Acad. Sci. U.S.A.* **1992**, *89*, 613−617.
(6) Vos, M. H.; Rappaport, F.; Lambry, J.-C.; Breton, J.; Martin, J.-L. *Nature* **1993**, *363*, 320−325.
(7) Vos, M. H.; Jones, M. R.; Hunter, C. N.; Breton, J.; Lambry, J.-C.; Martin, J.-L. *Biochemistry* **1994**, *33*, 6750−6757.
(8) Vos, M. H.; Jones, M. R.; Hunter, C. N.; Breton, J.; Martin, J.-L. *Proc. Natl. Acad. Sci. U.S.A.* **1994**, *91*, 12701−12705.
(9) Stanley, R. J.; Boxer, S. G. *J. Phys. Chem.* **1995**, *99*, 859−863.
(10) Vos, M. H.; Jones, M. R.; Martin, J. L. *Chem. Phys.* **1998**, *233*, 179−190.
(11) Yakovlev, A.; Shkuropatov, A.; Shuvalov, V. *FEBS Lett.* **2000**, *466*, 209−212.
(12) Yakovlev, A.; Shkuropatov, A.; Shuvalov, V. *Biochemistry* **2002**, *41*, 2667−2674.
(13) Yakovlev, A.; Shkuropatov, A.; Shuvalov, V. *Biochemistry* **2002**, *41*, 14019−14027.
(14) Shuvalov, V.; Yakovlev, A. *FEBS Lett.* **2003**, *540*, 26−34.
(15) Spörlein, S.; Zinth, W.; Wachtveitl, J. *J. Phys. Chem. B* **1998**, *102*, 7492−7496.
(16) Huppmann, P.; Spörlein, S.; Bibikova, M.; Oesterhelt, D.; Wachtveitl, J.; Zinth, W. *J. Phys. Chem. A* **2003**, *107*, 8302−8309.
(17) Palaniappan, V.; Aldema, M. A.; Frank, H. A.; Bocian, D. F. *Biochemistry* **1992**, *31*, 11050−11058.
(18) Czarnecki, K.; Diers, J. R.; Chynwat, V.; Erickson, J. P.; Frank, H. A.; Bocian, D. F. *J. Am. Chem. Soc.* **1997**, *119*, 415−426.
(19) Thompson, M. A.; Zerner, M. C.; Fajer, J. *J. Phys. Chem.* **1990**, *94*, 3820−3828.
(20) Thompson, M. A.; Zerner, M. C.; Fajer, J. *J. Phys. Chem.* **1991**, *95*, 5693−5700.
(21) Vos, M. H.; Martin, J.-L. *Biochim. Biophys. Acta* **1999**, *1411*, 1−20.
(22) Brooks, C. L., III; Karplus, M.; Pettitt, B. M. *Proteins: a Theoretical Perspective of Dynamics, Structure, and Thermodynamics*; John Wiley and Sons: New York, 1988.
(23) Peticolas, W. L. *Methods Enzymol.* **1978**, *61*, 425−458.
(24) Vos, M. H.; Jones, M. R.; Breton, J.; Lambry, J.-C.; Martin, J.-L. *Biochemistry* **1996**, *35*, 2687−2692.
(25) Savikhin, S.; Struve, W. S. *Biophys. J.* **1994**, *67*, 2002−2007.
(26) Chachisvilis, M.; Fidder, H.; Pullerits, T.; Sundström, V. *J. Raman Spectrosc.* **1995**, *26*, 513−522.
(27) Rischel, C.; Spiedel, D.; Ridge, J. P.; Jones, M. R.; Breton, J.; Lambry, J.-C.; Martin, J.-L.; Vos, M. H. *Proc. Natl. Acad. Sci. U.S.A.* **1998**, *95*, 12306−12311.
(28) Lotshaw, W. T.; McMorrow, D.; Thantu, N.; Melinger, J. S.; Kitchenbaum, R. *J. Raman Spectrosc.* **1995**, *26*, 571−583.
(29) McMorrow, D.; Lotshaw, W. T. *Chem. Phys. Lett.* **1993**, *201*, 369−376.
(30) McMorrow, D.; Lotshaw, W. T. *J. Phys. Chem.* **1991**, *95*, 10395−10406.
(31) Shelly, K. R.; Carson, E. A.; Beck, W. F. *J. Am. Chem. Soc.* **2003**, *125*, 11810−11811.
(32) Lakowicz, J. R. *Principles of Fluorescence Spectroscopy*, 2nd ed.; Kluwer Academic/Plenum Publishers: New York, 1999.
(33) Lampa-Pastirk, S.; Lafuente, R. C.; Beck, W. F. *J. Phys. Chem. B* **2004**, *108*, 12602−12607.
(34) Fragnito, H. L.; Bigot, J.-Y.; Becker, P. C.; Shank, C. V. *Chem. Phys. Lett.* **1989**, *160*, 101−104.
(35) Pollard, W. T.; Brito Cruz, C. H.; Shank, C. V.; Mathies, R. A. *J. Chem. Phys.* **1989**, *90*, 199−208.
(36) Pollard, W. T.; Fragnito, H. L.; Bigot, J.-Y.; Shank, C. V.; Mathies, R. A. *Chem. Phys. Lett.* **1990**, *168*, 239−245.
(37) Schoenlein, R. W.; Peteanu, L. A.; Mathies, R. A.; Shank, C. V. *Science* **1991**, *254*, 412−415.
(38) Dexheimer, S. L.; Wang, Q.; Peteanu, L. A.; Pollard, W. T.; Mathies, R. A.; Shank, C. V. *Chem. Phys. Lett.* **1992**, *188*, 61−66.
(39) Pollard, W. T.; Dexheimer, S. L.; Wang, Q.; Peteanu, L. A.; Shank, C. V.; Mathies, R. A. *J. Phys. Chem.* **1992**, *96*, 6147−6158.
(40) Peteanu, L. A.; Schoenlein, R. W.; Wang, Q.; Mathies, R. A.; Shank, C. V. *Proc. Natl. Acad. Sci. U.S.A.* **1993**, *90*, 11762−11766.
(41) Schoenlein, R. W.; Peteanu, L. A.; Wang, Q.; Mathies, R. A.; Shank, C. V. *J. Phys. Chem.* **1993**, *97*, 12087−12092.
(42) Wang, Q.; Schoenlein, R. W.; Peteanu, L. A.; Mathies, R. A.; Shank, C. V. *Science* **1994**, *266*, 422−424.
(43) Zhu, L.; Li, P.; Huang, M.; Sage, J. T.; Champion, P. M. *Phys. Rev. Lett.* **1994**, *72*, 301−304.
(44) Wang, W.; Demidov, A.; Ye, X.; Christian, J. F.; Sjodin, T.; Champion, P. M. *J. Raman Spectrosc.* **2000**, *31*, 99−105.
(45) Rosca, F.; Ionascu, D.; Kumar, A. T. N.; Demidov, A. A.; Champion, P. M. *Chem. Phys. Lett.* **2001**, *337*, 107−116.
(46) Diffey, W. M.; Beck, W. F. *Rev. Sci. Instrum.* **1997**, *68*, 3296−3300.
(47) Carson, E. A.; Diffey, W. M.; Shelly, K. R.; Lampa-Pastirk, S.; Dillman, K. L.; Schleicher, J. M.; Beck, W. F. *J. Phys. Chem. A* **2004**, *108*, 1489−1500.
(48) Evans, T.; Katz, J. *Biochim. Biophys. Acta* **1975**, *396*, 414−426.
(49) Katz, J.; Strain, H.; Leussing, D.; Dougherty, R. *J. Am. Chem. Soc.* **1968**, *90*, 784−791.
(50) Shipman, L.; Cotton, T. M.; Norris, J. R.; Katz, J. *J. Am. Chem. Soc.* **1976**, *98*, 8222−8230.
(51) Cantor, C. R.; Schimmel, P. R. *Biophysical Chemistry. Part II: Techniques for the Study of Biological Structure and Function*; W. H. Freeman and Company: San Francisco, CA, 1980.
(52) McHale, J. L. *Molecular Spectroscopy*; Prentice Hall: Upper Saddle River, NJ, 1999.
(53) Pollard, W. T.; Mathies, R. A. *Annu. Rev. Phys. Chem.* **1992**, *43*, 497−523.
(54) Balk, M. W.; Fleming, G. R. *J. Chem. Phys* **1985**, *83*, 4300−4307.
(55) Engh, R. A.; Petrich, J. W.; Fleming, G. R. *J. Phys. Chem.* **1985**, *89*, 618−621.
(56) Cong, P.; Deuhl, H. P.; Simon, J. D. *Chem. Phys. Lett.* **1993**, *211*, 367−373.
(57) Joo, T.; Jia, Y.; Yu, J.-Y.; Lang, M. J.; Fleming, G. R. *J. Chem. Phys.* **1996**, *104*, 6089−6108.
(58) Xu, Q.-H.; Ma, Y.-Z.; Stiopkin, I. V.; Fleming, G. R. *J. Chem. Phys.* **2002**, *116*, 9333−9340.
(59) Rector, K. D.; Zimdars, D.; Fayer, M. D. *J. Chem. Phys.* **1998**, *109*, 5455−5465.
(60) Siano, D. B.; Metzler, D. E. *J. Chem. Phys.* **1969**, *51*, 1856−1861.
(61) *pro Fit 6.0*; QuantumSoft: Uetikon am See, Switzerland.
(62) Weast, R. C. *CRC Handbook of Chemistry and Physics*, 85th ed.; CRC Press: Boca Raton, FL, 2004.
(63) McMorrow, D.; Lotshaw, W. T. *Chem. Phys. Lett.* **1990**, *174*, 85−94.
(64) McMorrow, D.; Lotshaw, W. T. *Chem. Phys. Lett.* **1991**, *178*, 69−74.
(65) McMorrow, D. *Opt. Commun.* **1991**, *86*, 236−244.
(66) Lotshaw, W. T.; Staver, P. R.; McMorrow, D.; Thantu, N.; Melinger, J. S. In *Ultrafast Phenomena IX*; Barbara, P. F., Knox, W. H., Mourou, G. A., Zewail, A. H., Eds.; Springer-Verlag: Berlin, 1994; pp 91−92.
(67) Castner, E. W.; Maroncelli, M. *J. Mol. Liq.* **1998**, *77*, 1−36.
(68) McMorrow, D.; Thantu, N.; Kleiman, V.; Melinger, J. S. *J. Phys. Chem. A* **2001**, *105*, 7960−7972.
(69) Albrecht, A. C. *J. Chem. Phys.* **1960**, *33*, 156−169.
(70) Tang, J.; Albrecht, A. C. In *Raman Spectroscopy: Theory and Practice*; Szymanski, H. A., Ed.; Plenum: New York, 1970; Vol. 2, pp 33−68.
(71) Albrecht, A. C.; Hutley, M. C. *J. Chem. Phys.* **1971**, *55*, 4438−4443.
(72) Myers, A. B.; Mathies, R. A. In *Biological Applications of Raman Spectroscopy*; Spiro, T. G., Ed.; Wiley-Interscience: New York, 1987; Vol. 2, *Resonance Raman Spectra of Polyenes and Aromatics*, pp 1−58.
(73) Lin, S. W.; Groesbeek, M.; van der Hoef, I.; Verdegem, P.; Lugtenburg, J.; Mathies, R. A. *J. Phys. Chem. B* **1998**, *102*, 2787−2806.
(74) Tauber, M. J.; Stuart, C. M.; Mathies, R. A. *J. Am. Chem. Soc.* **2004**, *126*, 3414−3415.
(75) Tauber, M. J.; Mathies, R. A. *Chem. Phys. Lett.* **2002**, *354*, 518−526.
(76) Alfano, J. C.; Walhout, P. K.; Kimura, Y.; Barbara, P. F. *J. Chem. Phys.* **1993**, *98*, 5996−5998.
(77) Kimura, Y.; Alfano, J. C.; Walhout, P. K.; Barbara, P. F. *J. Phys. Chem.* **1994**, *98*, 3450−3458.
(78) Reid, P. J.; Silva, C.; Walhout, P. K.; Barbara, P. F. *Chem. Phys. Lett.* **1994**, *228*, 658−664.
(79) Walhout, P. K.; Alfano, J. C.; Kimura, Y.; Silva, C.; Reid, P. J.; Barbara, P. F. *Chem. Phys. Lett.* **1995**, *232*, 135−140.
(80) Silva, C.; Walhout, P. K.; Reid, P. J.; Barbara, P. F. *J. Phys. Chem. A* **1998**, *102*, 5701−5707.
(81) Waterland, M.; Myers Kelley, A. *J. Chem. Phys.* **2000**, *113*, 6760−6773.
(82) Kambhampati, P.; Son, D. H.; Kee, T. W.; Barbara, P. F. *J. Phys. Chem. A* **2000**, *104*, 10637−10644.
(83) Jortner, J. *Z. Phys. D: At., Mol. Clusters* **1992**, *24*, 247−275.
(84) Spence, T. G.; Trotter, B. T.; Burns, T. D.; Posey, L. A. *J. Phys. Chem. A* **1998**, *102*, 6101−6106.
(85) Mikkelsen, K. V.; Ratner, M. A. *J. Chem. Phys.* **1989**, *90*, 4237−4247.
(86) Mikkelsen, K. V.; Ratner, M. A. *J. Phys. Chem.* **1989**, *93*, 1759−1770.
(87) Billing, G. D.; Mikkelsen, K. V. *Advanced Molecular Dynamics and Chemical Kinetics*; John Wiley & Sons: New York, 1997.
(88) Gamba, Z.; Klein, M. L. *J. Chem. Phys.* **1990**, *92*, 6973−6974.
(89) Wynne, K.; Galli, C.; Hochstrasser, R. M. *Chem. Phys. Lett.* **1992**, *193*, 17−22.

(90) Cox, E.; Cruickshank, D.; Smith, J. *Proc. R. Soc. A* **1958**, *247*, 1−21.
(91) Bacon, G.; Curry, N.; Wilson, S. *Proc. R. Soc. A* **1964**, *279*, 98−110.
(92) Park, Y. C.; Lee, J. S. *J. Phys. Chem. B* **2006**, *110*, 5091−5095.
(93) Tsuzuki, S.; Uchimaru, T.; Mikami, M. *J. Phys. Chem. A* **2006**, *110*, 2027−2033.
(94) Lee, N. K.; Park, S.; Kim, S. K. *J. Chem. Phys.* **2002**, *116*, 7902−7909.
(95) Lee, N. K.; Park, S.; Kim, S. K. *J. Chem. Phys.* **2002**, *116*, 7910−7917.
(96) Kincaid, J. R.; Proniewicz, L. M.; Bajdor, K.; Bruha, A.; Nakamoto, K. *J. Am. Chem. Soc.* **1985**, *107*, 6775−6781.
(97) Proniewicz, L. M.; Nakamoto, K.; Kincaid, J. R. *J. Am. Chem. Soc.* **1988**, *110*, 4541−4545.
(98) Ladanyi, B. M.; Stratt, R. M. *J. Phys. Chem.* **1995**, *99*, 2502−2511.
(99) Stratt, R. M.; Maroncelli, M. *J. Phys. Chem.* **1996**, *100*, 12981−12996.
(100) Garg, S. K.; Smyth, C. P. *J. Phys. Chem.* **1965**, *69*, 1294−1301.
(101) Jorgensen, W. L. *J. Am. Chem. Soc.* **1980**, *102*, 543−549.
(102) Bertolini, D.; Cassettari, M.; Salvetti, G. *J. Chem. Phys.* **1983**, *78*, 365−372.
(103) Sumi, H.; Marcus, R. A. *J. Chem. Phys.* **1986**, *84*, 4272−4276.
(104) London, F. *Trans. Faraday Soc.* **1937**, *33*, 8−26.
(105) Margenau, H. *Rev. Mod. Phys.* **1939**, *11*, 1−35.
(106) Kauzmann, W. *Quantum Chemistry: An Introduction*; Academic Press: New York, 1957.
(107) Berry, R. S.; Rice, S. A.; Ross, J. *Physical Chemistry*, 2nd ed.; Oxford University Press: New York, 2000.
(108) Berg, M.; Vanden Bout, D. A. *Acc. Chem. Res.* **1997**, *30*, 65−71.
(109) Berg, M. *J. Phys. Chem. A* **1998**, *102*, 17−30.
(110) Berg, M. *J. Chem. Phys.* **1999**, *110*, 8577−8588.